ARTICLE

Photoionization Mass Spectrometric and Kinetic Modeling of Low-pressure Pyrolysis of Benzene

Jiu-zhong Yang[a,b], Long Zhao[a], Jiang-huai Cai[a], Fei Qi[a,b], Yu-yang Li [b*]

a. National Synchrotron Radiation Laboratory, University of Science and Technology of China, Hefei 230029, China

b. State Key Laboratory of Fire Science, University of Science and Technology of China, Hefei 230029, China

(Dated: Received on March 7, 2013; Accepted on April 7, 2013)

Pyrolysis of benzene at 30 Torr was studied from 1360 K to 1820 K in this work. Synchrotron vacuum ultraviolet photoionization mass spectrometry was employed to detect the pyrolysis products such as radicals, isomers and polycyclic aromatic hydrocarbons, and measure their mole fraction profiles versus temperature. A low-pressure pyrolysis model of benzene was developed and validated by the experimental results. Rate of production analysis was performed to reveal the major reaction networks in both fuel decomposition and aromatic growth processes. It is concluded that benzene is mainly decomposed via H-abstraction reaction to produce phenyl and partly decomposed via unimolecular decomposition reactions to produce propargyl or phenyl. The decomposition process stops at the formation of acetylene and polyyne species like diacetylene and 1,3,5-hexatriyne due to their high thermal stabilities. Besides, the aromatic growth process in the low-pressure pyrolysis of benzene is concluded to initiate from benzene and phenyl, and is controlled by the even carbon growth mechanism due to the inhibited formation of C5 and C7 species which play important roles in the odd carbon growth mechanism.

Key words: Benzene, Low-pressure pyrolysis, PAH formation, Synchrotron vacuum ultraviolet photoionization mass spectrometry, Kinetic model

I. INTRODUCTION

Petroleum-derived oils like gasoline, diesel oil and kerosene are principal sources of transportation fuels nowadays, and will still play key roles in transportation field in foreseeable future. However, the limited reserves and the rapidly increasing demand of petroleum are in extraordinarily strong conflict, which requires our attention on more effective combustion of petroleum-derived oils. On the other hand, the combustion of transportation fuels emits great amount of air pollutants such as NO_x, polycyclic aromatic hydrocarbons (PAHs) and soot, and leads to serious environment and health problems [1−3]. To solve these problems, better understanding of combustion chemistry of petroleum-derived oils is required.

Aromatic hydrocarbons are one of the major component families in petroleum-derived oils [4−6] and are broadly used as major components in the surrogates of transportation fuels [7, 8]. Aromatics are also frequently used as gasoline additives to improve the antiknocking performance and antioxidative stability of gasoline. Compared with paraffins and olefins with the same carbon atoms, aromatics usually have higher boiling points and heavier sooting tendencies, which hinder the experimental investigation of aromatic combustion.

With the simplest molecular structure and lowest boiling point among all aromatics, benzene (C_6H_6) is a prototypical aromatic fuel in combustion studies. Though the combustion of benzene has been extensively studied, most previous experimental work focused on the oxidation and flames, while only a few groups studied the pyrolysis [9−12]. Laser spectroscopic techniques were used to investigate the soot formation in shock tube pyrolysis of benzene [9, 10]. Among the work providing product concentration data, gas chromatography (GC) is the commonest diagnostic technique. In 1996, Laskin and Lifshitz studied the thermal decomposition of benzene in a shock tube at the pressure of ∼0.8 atm and temperature range of 1400−2000 K, and detected 6 stable products using GC [11]. In 2006, Sivaramakrishnan *et al.* also used GC techniques to study the pyrolysis of benzene in a shock tube at pressures of 30 and 50 bar and high temperature range of 1200−1800 K and also detected six stable products [12]. However, it is recognized that GC techniques can hardly detect reactive intermediates, especially radicals, due to the high

*Author to whom correspondence should be addressed. E-mail: yuygli@ustc.edu.cn, Tel.: +86-551-63607923, FAX: +86-551-65141078

operation pressure and long retention time [3].

In this work, the pyrolysis of benzene was studied in a flow reactor at 30 Torr. Synchrotron vacuum ultraviolet photoionization mass spectrometry (SVUV-PIMS) was employed to detect pyrolysis species, and provides the possibility to investigate radicals. Furthermore, a low-pressure pyrolysis model of benzene was developed from our previous combustion models of aromatics and validated by the experimental results in this work.

II. EXPERIMENTS

The experiment was performed at National Synchrotron Radiation Laboratory, Hefei, China. The pyrolysis apparatus has been described in our previous work [13−16]. In brief, it consists of a pyrolysis chamber, a differentially pumped chamber and a photoionization chamber with a home-made reflectron time-of-flight mass spectrometer (RTOF-MS). The flow reactor in the pyrolysis chamber is composed of a 6.8-mm-inner-diameter alumina flow tube heated by an electric furnace. The heating length of the flow tube is 15.0 cm. The sampling and detection procedures can be found elsewhere [13−16].

Benzene with a purity of ≥99.5% was purchased from Shanghai Aladdin Reagent Co., Ltd., China, and argon (Ar) with a purity of ≥99.99% was provided by Nanjing Special Gas Co., Ltd., China. The liquid flow rate of benzene was controlled by a liquid chromatography pump (Zhejiang Fuli Analytical Instrument Co., Ltd., China). The gas flow rate of argon was controlled by a mass flow controller (MKS Instruments, Inc., USA). Benzene was vaporized and perfectly mixed with argon before entering the flow tube. The flow rates of Ar and benzene in gas phase are 0.975 and 0.025 standard liters per minute (SLM), respectively. The mass flow rate is 0.0837 g/(cm^2s), and the pressure is 30 Torr.

The experiment was carried out at the temperature ranging from 1360 K to 1820 K, while the pressure in the pyrolysis chamber was maintained at 30 Torr. The methods of axial temperature measurement and pressure calculation were introduced in detail previously [14] and will not be repeated here. The uncertainties of measured temperatures are within ±30 K. The experiment was conducted with two modes: (i) mass spectra were recorded at a fixed pyrolysis temperature with various photon energies to measure the photoionization efficiency (PIE) spectra which provide information of ionization energies (IEs) for species identification; (ii) mass spectra were recorded at some fixed photon energies with various pyrolysis temperatures to measure mole fraction profiles of pyrolysis species versus temperatures. The photoionization cross section (PICS) data of most detected species are available in the online database [17]. The experimental uncertainties of mole fractions are evaluated to be ±25% for products with known PICS data and a factor of 2 for those with estimated PICS data.

III. KINETIC MODELING

Based on our previous models of toluene and ethylbenzene [18, 19], a new low-pressure pyrolysis model of benzene including 140 species and 474 reactions was constructed in this work. Table I lists the rate constants of some important reactions in Arrhenius form $k=AT^n e^{-E_a/RT}$. The model consists of two parts, *i.e.* the decomposition submechanism of benzene and the formation submechanism of large aromatics. The decomposition submechanism of benzene is mainly taken from our previous aromatic models [18, 19]. In benzene pyrolysis, H-abstraction of benzene by H attack is vital for the consumption of benzene. In this work, the calculated results by Barckholtz *et al.* [20] were employed, as listed in Table I. Besides, the unimolecular decomposition reactions of benzene [21, 22] and further decomposition reactions of phenyl and benzyne [24−26] are also included. The formation submechanism of large aromatics is mainly referred to the hydrogen-abstraction-carbon-addition (HACA) mechanism by Wang and Frenklach [26], the model of surrogate fuels by Blanquart *et al.* [27] and the low-pressure benzene model by Richter *et al.* [28]. For the reactions without available literature rate constants, their rate constants were estimated from analogous reactions.

The simulation was carried out with the Plug Flow Reactor (PFR) code in the CHEMKIN-Pro Software [29]. Detailed description of the simulation method can be found in our previous work [14].

IV. RESULTS AND DISCUSSION

The pyrolysis of an aromatic fuel is composed of two major processes, *i.e.* the decomposition of fuel and the formation of large aromatics. Figure 1 shows the mass spectra recorded at 1820 K and various photon energies. For each mass spectrum, the ion intensities have been weighted by the measured photon flux. Large aromatics can be observed at quite low photon energies such as 9.00 eV due to their low ionization energies, while mass peaks of benzene (m/z=78) and its decomposition products emerge gradually as the photon energy increases. Based on the modeling results, rate of production (ROP) analysis was performed to reveal the main reaction pathways in the two processes of low-pressure benzene pyrolysis. Since most products were observed with relatively high concentrations at around 1750 K, this temperature was chosen to perform the ROP analysis. Among the species with experimental and predicted results shown in the following figures, benzyne (C_6H_4), naphthalene ($C_{10}H_8$), biphenyl ($C_{12}H_{10}$), acenaphthylene ($C_{12}H_8$), and phenanthrene ($C_{14}H_{10}$) do not have

DOI:10.1063/1674-0068/26/03/245-251

TABLE I The important reactions in the low-pressure pyrolysis model of benzene.

Order	Reaction	A	n	E/(kcal/mol)	Reference
1	$C_6H_6+H=C_6H_5+H_2$	1.60×10^{11}	1.08	10395.40	[20]
2	$C_6H_5+H=C_6H_6$	8.02×10^{19}	−2.00	1968.00	[21]
3	$C_3H_3+C_3H_3=C_6H_6$ duplicate	1.64×10^{66}	−15.90	27529.00	[22]
		1.20×10^{35}	−7.40	5058.00	[22]
4	$C_6H_5=C_6H_4+H$	5.00×10^{12}	0.00	72923.00	[23][a]
5	$C_3H_3+C_3H_3=C_6H_5+H$	8.00×10^{53}	−11.94	28973.00	[24][b]
6	$C_6H_4=C_4H_2+C_2H_2$	2.00×10^{14}	0.00	83000.00	[25][c]
7	$C_6H_6+C_2H=C_8H_6+H$	5.00×10^{13}	0.00	0.00	[26]
8	$C_6H_5+C_2H_2=C_8H_6+H$	7.50×10^{26}	−4.00	16000.00	[26]
9	$C_6H_6+C_4H_3=C_{10}H_8+H$	5.00×10^{11}	0.00	0.00	[d]
10	$C_{10}H_8+H=C_{10}H_7+H_2$	2.50×10^{14}	0.00	0.00	[26]
11	$C_{10}H_7+H(M)=C_{10}H_8(M)$	1.00×10^{14}	0.00	0.00	[26]
	Low/	3.80×10^{127}	−31.43	18676.00/	
	TROE/0.200	122.80	478.40	5411.90/	
12	$C_6H_6+C_6H_5=C_{12}H_{10}+H$	4.10×10^{43}	−9.20	15153.00	[26]
13	$C_9H_7+C_3H_3=C_{12}H_8+H_2$	1.50×10^{75}	−17.80	39600.00	[27]
14	$C_9H_7+C_3H_2=C_{12}H_8+H$	1.00×10^{12}	0.00	0.00	[d]
15	$C_6H_5+C_6H_5C_2H=C_{14}H_{10}+H$	1.10×10^{23}	−2.90	15890.00	[26]
16	$C_6H_6+C_8H_5=C_{14}H_{10}+H$	1.10×10^{23}	−2.90	15890.00	[26]

[a] Divided by a factor of 6 with consideration of the fall-off effect of reaction rate at low pressure.
[b] Divided by a factor of 2.
[c] Divided by a factor of 3.25 with consideration of the fall-off effect of reaction rate at low pressure.
[d] Estimated from the rate constants of analogous reactions.

available PICS data. Therefore their experimental uncertainties are estimated to be a factor of 2.

A. Decomposition of benzene

Figures 2 and 3 display the experimental and predicted mole fraction profiles of benzene, argon and several decomposition products. To guide the eye, the reaction network of benzene decomposition at 1750 K is drawn in Fig.4 based on the ROP analysis. Figure 2 presents the experimental and predicted mole fraction profiles of benzene, C_6H_4, Ar, and H_2 versus temperature. The mole fraction of Ar keeps constant at 0.975 before 1550 K and drops slightly afterward. Since Ar is chemically inert and has invariable mole number during the experiment, the decrease of its mole fraction indicates the increase of total mole number of sampled gases due to the decay of benzene to smaller products.

Benzene starts to decompose at about 1550 K and is almost three fourths consumed at 1820 K. The ROP analysis indicates that about 80% benzene is decomposed to smaller products, while the rest combines with C2-C6 products to produce large aromatics. H-abstraction by H attack (Reaction (1)) to produce phenyl radical (C_6H_5) is the dominant decomposition pathway of benzene at 1750 K and consumes more than 60% of benzene, while the unimolecular decomposition reactions of benzene (Reactions (2) and (3)) only contribute less than 20% for the consumption of benzene. This is because H radical is abundantly produced in the reactions of pyrolysis products at 1750 K. Furthermore, R1 is also the most important source of hydrogen.

$$C_6H_6 + H = C_6H_5 + H_2 \quad (1)$$
$$C_6H_5 + H = C_6H_6 \quad (2)$$
$$C_3H_3 + C_3H_3 = C_6H_6 \quad (3)$$

As the most important primary decomposition product, phenyl attracts almost 70% reaction flux from benzene (Reactions (1) and (2)). However, the resonantly stabilized structure of benzene is destroyed during the break of C−H bond, resulting in the rapid consumption rate and negligible concentration level of phenyl due to its unstable molecular structure. Decomposition of phenyl mainly leads to the formation of benzyne, and part of phenyl is converted to propargyl radical (C_3H_3).

$$C_6H_5 = C_6H_4 + H \quad (4)$$
$$C_3H_3 + C_3H_3 = C_6H_5 + H \quad (5)$$

Since benzyne is the dominant product of phenyl and can be observed in this work, it can serve as the indicator of phenyl. Though the experimental uncertainty of its mole fractions is quite large due to the unknown

DOI:10.1063/1674-0068/26/03/245-251

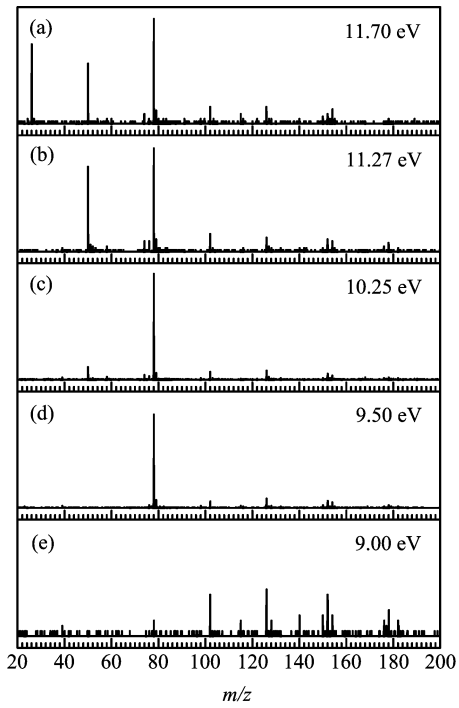

FIG. 1 Photon-flux-weighted mass spectra recorded at 1820 K and different photon energies. To keep the same Y axis scale at all conditions, the region of m/z=77−80 is divided by 2 in (a) and (b), and the total mass spectrum is multiplied by 2 and 20 in (d) and (e), respectively.

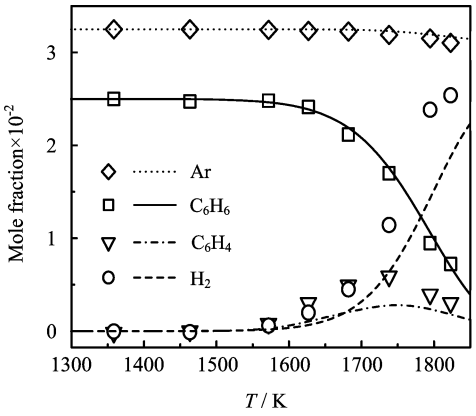

FIG. 2 Experimental (symbols) and predicted (lines) mole fraction profiles of C_6H_6, C_6H_4, Ar, and H_2.

PICS data, the good accordance in the formation temperature and peak temperature between the predicted and experimental results still validates the performance of reactions involving phenyl. Because the triple-bond leads to great tension of the ring structure, benzyne can be readily decomposed via ring-opening reaction to form C_4H_2 and C_2H_2 (Reaction (6)).

$$C_6H_4 = C_4H_2 + C_2H_2 \quad (6)$$

Figure 3 presents the experimental and predicted

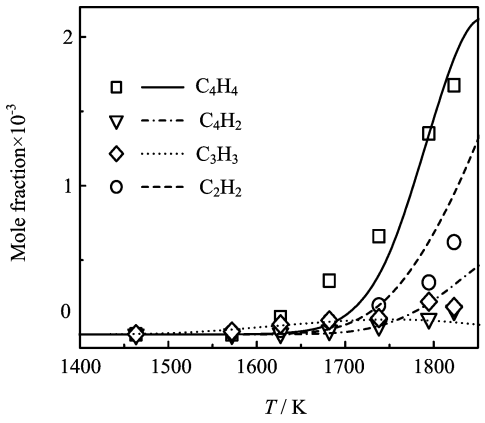

FIG. 3 Experimental (symbols) and predicted (lines) mole fraction profiles of C_4H_4, C_4H_2, C_3H_3, and C_2H_2.

mole fraction profiles of vinylacetylene (C_4H_4), diacetylene (C_4H_2), propargyl radical (C_3H_3), and acetylene (C_2H_2). Diacetylene is one of the most abundant pyrolysis products in both this work and previous benzene pyrolysis studies [11, 12], because it is produced from the main decomposition reaction sequence of benzene ($C_6H_6 \rightarrow C_6H_5 \rightarrow C_6H_4 \rightarrow C_4H_2 + C_2H_2$), and also due to its high thermal stability [30]. As a result, its mole fraction is much higher than that of vinylacetylene, as shown in Fig.3. The stable structure of diacetylene also limits its further decomposition. Only 30% of formed diacetylene can be consumed, mainly via combination reactions to form large aromatics and H attack reaction to produce acetylene and ethynyl radical. Similarly to diacetylene, acetylene also attracts great reaction flux and accumulates high concentrations in both this work and previous work of benzene pyrolysis [11, 12].

Propargyl radical is the other important primary product from benzene decomposition, and also attracts part of reaction flux from phenyl. Almost all propargyl comes from Reactions (3) and (5). Benefitting from the application of SVUV-PIMS, propargyl was unambiguously detected in this work. Its decay is controlled by the formation of triplet propargylene (C_3H_2) via either unimolecular C−H scission or H-abstraction by H attack. The consumption of triplet propargylene is dominated by combination reactions to form larger species, such as vinylacetylene and 1,3,5-hexatriyne, as shown in Fig.4.

In a word, the decomposition of benzene at low pressure mainly forms phenyl via H-abstraction reaction by H attack, and partly produces propargyl or phenyl via unimolecular decomposition reactions, and stops at acetylene and polyyne species such as diacetylene and 1,3,5-hexatriyne due to their extraordinarily high thermal stabilities at high temperatures [30]. Furthermore, it is noticed that C5 and C1 products were not observed in this work because the decomposition pathways from benzene to these products are very difficult to proceed in pyrolysis circumstance. This phenomenon leads to

DOI:10.1063/1674-0068/26/03/245-251

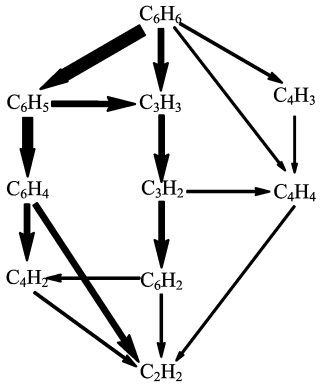

FIG. 4 Reaction network of benzene decomposition at 1750 K. Thickness of each arrow represents the flux of corresponding reaction.

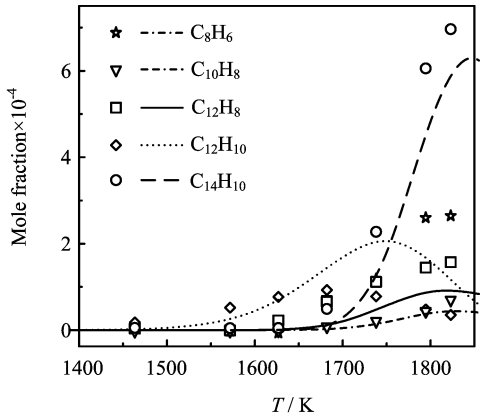

FIG. 5 Experimental (symbols) and predicted (lines) mole fraction profiles of C_8H_6, $C_{10}H_8$, $C_{12}H_8$, $C_{12}H_{10}$ and $C_{14}H_{10}$.

remarkable influences on the aromatic growth process, and will be discussed in detail below.

B. Formation of large aromatics

In this work, several large aromatics including C7-C8 monocyclic aromatic hydrocarbons (MAHs) and PAHs with 2−4 rings were detected. Figure 5 shows the experimental and predicted mole fraction profiles of several typical large aromatics including phenylacetylene (C_8H_6), naphthalene ($C_{10}H_8$), acenaphthylene ($C_{12}H_8$), biphenyl ($C_{12}H_{10}$), and phenanthrene ($C_{14}H_{10}$). To guide the eye, the reaction network of aromatic growth at 1750 K is drawn in Fig.6 based on the ROP analysis.

As summarized in our previous work [18, 31], there are two major aromatic growth mechanisms. The even carbon growth mechanism includes addition reactions of species with even carbon atoms to certain precursors, especially the HACA mechanism with sequential addition reactions of C2 or C4 species (*e.g.* acetylene, vinylacetylene, and their radicals) [26]. The other one is the odd carbon growth mechanism. It mainly consists of addition reactions of C3 or C5 resonantly stabilized radicals to certain precursors like cyclopentadienyl radical (C_5H_5) and benzyl radical (C_7H_7) [32, 33]. Based on the following discussion, the contributions of two mechanisms in the aromatic growth process of low-pressure benzene pyrolysis will be evaluated.

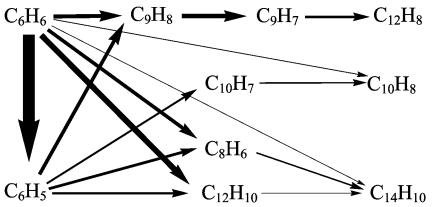

FIG. 6 Reaction network of aromatic growth at 1750 K. Thickness of each arrow represents the flux of corresponding reaction and is in different scale as the arrow thicknesses in Fig.4.

Among MAHs, C7 products such as toluene and benzyl were only observed with very low concentration levels (even lower than many PAHs) because their formation relies on methyl radical (CH_3) which was not observed in this work, implying their negligible roles in the aromatic growth process. Among C8 MAHs, phenylacetylene is an important precursor of PAHs due to its highly unsaturated molecular structure. The ROP analysis indicates that phenylacetylene mainly comes from the reactions of benzene with ethynyl (Reaction (7)) and phenyl with acetylene (Reaction (8)) which are typical HACA pathways.

$$C_6H_6 + C_2H = C_6H_5C_2H + H \quad (7)$$

$$C_6H_5 + C_2H_2 = C_6H_5C_2H + H \quad (8)$$

Naphthalene is one of the smallest PAHs, and its formation is broadly accepted as the start point of PAH formation [3]. There are a number of possible formation pathways of naphthalene, especially C5+C5, C6+C4 and C7+C3 pathways [3]. In this work, the dominant pathways of naphthalene formation (Reactions (9)−(11)) can be summarized as C6+C4 pathways which are also HACA pathways, since 1-naphthyl radical ($C_{10}H_7$) is the combination product of phenyl and diacetylene. On the other hand, the odd carbon growth mechanism such as C5+C5 and C7+C3 pathways cannot compete with HACA pathways in the low-pressure pyrolysis of benzene, due to the inhibited formation of key C5 and C7 products such as cyclopentadienyl radical and benzyl radical as mentioned before.

$$C_6H_6 + C_4H_3 = C_{10}H_8 + H \quad (9)$$

$$C_{10}H_8 + H = C_{10}H_7 + H_2 \quad (10)$$

$$C_{10}H_7 + H(M) = C_{10}H_8(M) \quad (11)$$

Biphenyl ($C_{12}H_{10}$) and acenaphthylene ($C_{12}H_8$) are two observed C12 species in this work. As observed

DOI:10.1063/1674-0068/26/03/245-251

from Fig.5, biphenyl is formed at much lower temperature and has higher peak mole fraction than other large aromatics, indicating its significant role in benzene consumption. In fact, biphenyl is almost totally formed from the reaction of benzene with phenyl (Reaction (12)) which can also be classified into the even carbon growth mechanism. Different from above-mentioned three large aromatics, acenaphthylene is a typical product by C3-addition pathways which belong to the odd carbon growth mechanism. Its main formation pathways (Reactions (13) and (14)) are the addition reactions of C3 radicals to indenyl radical (C_9H_7) which mainly comes from the C3 radical addition to benzene or phenyl, as shown in Fig.6.

$$C_6H_6 + C_6H_5 = C_{12}H_{10} + H \quad (12)$$

$$C_9H_7 + C_3H_3 = C_{12}H_8 + H_2 \quad (13)$$

$$C_9H_7 + C_3H_2 = C_{12}H_8 + H \quad (14)$$

Phenanthrene ($C_{14}H_{10}$) is one of the most important tricyclic PAHs. Its main formation pathways in this work can be classified into two kinds, *i.e.* C6+C8 and C12+C2 pathways, which both belong to the even carbon growth mechanism. The C6+C8 pathways (Reactions (15) and (16)) including reactions of phenyl with phenylacetylene and benzene with phenylethynyl radical contribute about 75% to the formation of phenanthrene, while the C12+C2 pathways including reactions of C2 species with biphenyl and its radical contribute almost 20%.

$$C_6H_5 + C_6H_5C_2H = C_{14}H_{10} + H \quad (15)$$

$$C_6H_6 + C_8H_5 = C_{14}H_{10} + H \quad (16)$$

Based on above discussions, it is summarized that benzene and phenyl are dominant PAH precursors in the low-pressure pyrolysis of benzene. Between the two major formation mechanisms of large aromatics, the even carbon growth mechanism is concluded to be the controlling mechanism of aromatic growth in this work due to the inhibited production of C5 and C7 species. The only important odd carbon growth pathway is the sequentially C3-addition reactions on benzene or phenyl to produce acenaphthylene.

V. CONCLUSION

The pyrolysis of benzene at 30 Torr was studied in a flow reactor with SVUV-PIMS. A number of pyrolysis species were detected, and their mole fractions were quantified. Based on the validation by experimental results, a low-pressure pyrolysis model of benzene was developed from our previous aromatic models. The decomposition of benzene mainly forms phenyl and propargyl initially, and stops at the formation of acetylene and polyyne species. The aromatic growth process is mainly initiated by reactions involving benzene and phenyl, and is controlled by the even carbon growth mechanism since the odd carbon growth mechanism is inhibited by the low concentration levels of C5 and C7 products.

VI. ACKNOWLEDGEMENTS

This work is supported by the National Natural Science Foundation of China (No.51106146 and No.51036007), China Postdoctoral Science Foundation (No.20100480047 and No.201104326), Chinese Universities Scientific Fund (No.WK2310000010), and Chinese Academy of Sciences.

[1] H. Richter and J. B. Howard, Prog. Energy Combust. Sci. **26**, 565 (2000).
[2] K. Siegmann and H. C. Siegmann, *Molecular Precursor of Soot and Quantification of the Associated Health Risk*, J. L. Morán-Lćpez Ed. *Current Problems in Condensed Matter*, New York: Plenum Press, (1998).
[3] C. S. McEnally, L. D. Pfefferle, B. Atakan, and K. Kohse-Höinghaus, Prog. Energy Combust. Sci. **32**, 247 (2006).
[4] J. Wang, B. Yang, Y. Y. Li, Z. Y. Tian, T. C. Zhang, F. Qi, and K. Nakajima, Int. J. Mass Spectrom. **263**, 30 (2007).
[5] J. T. Farrell, N. P. Cernansky, F. L. Dryer, C. K. Law, D. G. Friend, C. A. Hergart, R. M. McDavid, A. K. Patel, C. J. Mueller, and H. Pitsch, *Development of an Experimental Database and Kinetic Models for Surrogate Diesel Fuels*, SAE Paper 2007-01-0201, Society of Automotive Engineers, (2007).
[6] O. J. Hadaller and J. M. Johnson, *World Fuel Sampling Program*, CRC Report No. 647, Coordinating Research Council, Inc., (2006).
[7] A. Violi, S. Yan, E. G. Eddings, F. Sarofim, S. Granata, T. Faravelli, and E. Ranzi, Combust. Sci. Technol. **174**, 399 (2002).
[8] W. J. Pitz and C. J. Mueller, Prog. Energy Combust. Sci. **37**, 330 (2011).
[9] R. Starke and P. Roth, Combust. Flame **127**, 2278 (2001).
[10] G. Agafonov, P. Vlasov, and V. Smirnov, Kinet. Catal. **52**, 358 (2011).
[11] A. Laskin and A. Lifshitz, Proc. Combust. Inst. **26**, 669 (1996).
[12] R. Sivaramakrishnan, K. Brezinsky, H. Vasudevan, and R. S. Tranter, Combust. Sci. Technol. **178**, 285 (2006).
[13] Y. Y. Li, L. D. Zhang, T. Yuan, K. W. Zhang, J. Z. Yang, B. Yang, F. Qi, and C. K. Law, Combust. Flame **157**, 143 (2010).
[14] Y. J. Zhang, J. H. Cai, L. Zhao, J. Z. Yang, H. F. Jin, Z. J. Cheng, Y. Y. Li, L. D. Zhang, and F. Qi, Combust. Flame **159**, 905 (2012).
[15] Y. Y. Li, L. D. Zhang, Z. D. Wang, L. L. Ye, J. H. Cai, Z. J. Cheng, and F. Qi, Proc. Combust. Inst. **34**, 1739 (2013).
[16] F. Qi, Proc. Combust. Inst. **34**, 33 (2013).

DOI:10.1063/1674-0068/26/03/245-251

[17] National Synchrotron Radiation Laboratory, *Photonionization Cross Section Database (Version 1.0)*, Hefei: University of Science and Technology, (2013), http://flame.nsrl.ustc.edu.cn/en/database.htm.
[18] Y. Y. Li, J. H. Cai, L. D. Zhang, T. Yuan, K. W. Zhang, and F. Qi, Proc. Combust. Inst. **33**, 593 (2011).
[19] Y. Y. Li, J. H. Cai, L. D. Zhang, J. Z. Yang, Z. D. Wang, and F. Qi, Proc. Combust. Inst. **33**, 617 (2011).
[20] C. Barckholtz, T. A. Barckholtz, and C. M. Hadad, J. Phys. Chem. A **105**, 140 (2000).
[21] A. M. Mebel, M. C. Lin, D. Chakraborty, J. Park, S. H. Lin, and Y. T. Lee, J. Chem. Phys. **114**, 8421 (2001).
[22] N. Hansen, T. A. Cool, P. R. Westmoreland, and K. Kohse-Höinghaus, Prog. Energy Combust. Sci. **35**, 168 (2009).
[23] L. K. Madden, L. V. Moskaleva, S. Kristyan, and M. C. Lin, J. Phys. Chem. A **101**, 6790 (1997).
[24] J. A. Miller and S. J. Klippenstein, J. Phys. Chem. A **107**, 7783 (2003).
[25] C. Xu, M. Braun-Unkhoff, C. Naumann, and P. Frank, Proc. Combust. Inst. **31**, 231 (2007).
[26] H. Wang and M. Frenklach, Combust. Flame **110**, 173 (1997).
[27] G. Blanquart, P. Pepiot-Desjardins, and H. Pitsch, Combust. Flame **156**, 588 (2009).
[28] H. Richter and J. B. Howard, Phys. Chem. Chem. Phys. **4**, 2038 (2002).
[29] *CHEMKIN-PRO 15092*, Reaction Design, San Diego (2009).
[30] A. V. Krestinin, Proc. Combust. Inst. **27**, 1557 (1998).
[31] Y. Y. Li, L. D. Zhang, Z. Y. Tian, T. Yuan, J. Wang, B. Yang, and F. Qi, Energy Fuels **23**, 1473 (2009).
[32] M. B. Colket and D. J. Seery, Proc. Combust. Inst. **25**, 883 (1994).
[33] C. F. Melius, M. E. Colvin, N. M. Marinov, W. J. Pitz, and S. M. Senkan, Proc. Combust. Inst. **26**, 685 (1996).

DOI:10.1063/1674-0068/26/03/245-251